The Global Character of the Flux of Downward Longwave Radiation

GRAEME L. STEPHENS,* MARTIN WILD,+ PAUL W. STACKHOUSE JR.,# TRISTAN L'ECUYER,@ SEIJI KATO,# AND DAVID S. HENDERSON@

* *Jet Propulsion Laboratory, California Institute of Technology, Pasadena, California*
+ *Institute for Atmospheric and Climate Science, ETH Zurich, Zurich, Switzerland*
# *NASA Langley Research Center, Hampton, Virginia*
@ *Department of Atmospheric Sciences, Colorado State University, Fort Collins, Colorado*

(Manuscript received 9 May 2011, in final form 12 September 2011)

ABSTRACT

Four different types of estimates of the surface downwelling longwave radiative flux (DLR) are reviewed. One group of estimates synthesizes global cloud, aerosol, and other information in a radiation model that is used to calculate fluxes. Because these synthesis fluxes have been assessed against observations, the global-mean values of these fluxes are deemed to be the most credible of the four different categories reviewed. The global, annual mean DLR lies between approximately 344 and 350 W m^{-2} with an error of approximately ± 10 W m^{-2} that arises mostly from the uncertainty in atmospheric state that governs the estimation of the clear-sky emission. The authors conclude that the DLR derived from global climate models are biased low by approximately 10 W m^{-2} and even larger differences are found with respect to reanalysis climate data. The DLR inferred from a surface energy balance closure is also substantially smaller that the range found from synthesis products suggesting that current depictions of surface energy balance also require revision. The effect of clouds on the DLR, largely facilitated by the new cloud base information from the *CloudSat* radar, is estimated to lie in the range from 24 to 34 W m^{-2} for the global cloud radiative effect (all-sky minus clear-sky DLR). This effect is strongly modulated by the underlying water vapor that gives rise to a maximum sensitivity of the DLR to cloud occurring in the colder drier regions of the planet. The bottom of atmosphere (BOA) cloud effect directly contrast the effect of clouds on the top of atmosphere (TOA) fluxes that is maximum in regions of deepest and coldest clouds in the moist tropics.

1. Introduction

It has been understood for some time that changes to the strength of the greenhouse effect are fundamental to our understanding of the climate of earth and how it can change (Arrenhius 1896; Callendar 1938; Kasting 1989). Increases in greenhouse gases like CO_2 induce a warming of the surface and lower atmosphere. The increase in water vapor that follows a warming results in a further strengthening of the greenhouse effect by increased emission of radiation from the atmosphere to the surface that induces even more warming. This is the essence of the positive water vapor feedback that occurs through the connections between temperature, water vapor, and emission of infrared radiation (e.g., Held and Soden 2000).

A common recent perception is the water vapor feedback is mostly defined by the changes to the upper-tropospheric water vapor that are conjectured to occur with warming because of the disproportionately greater influence of this water vapor on the emission of longwave radiation to space (Lindzen 1990; Stephens and Greenwald 1991; Held and Soden 2000). This has led to some debate about the magnitude and even the sign of this feedback in the real earth system given there is debate about how the upper-tropospheric water vapor has changed with the current warming (e.g., Paltridge et al. 2009; Soden et al. 2005). With this upper-tropospheric focus, the relative importance of the changes in water vapor that are expected to occur nearer the earth's surface, which is less controversial, tends to be overlooked (Shine and Sinha 1991). It is the increasing lower-level water vapor that occurs with warming (e.g., Santer et al. 2007), however, that is responsible for the increased emission of infrared radiation to the surface that fundamentally determines the surface warming (Garatt 2001).

Corresponding author address: Graeme L. Stephens, Jet Propulsion Laboratory, California Institute of Technology, 4800 Oak Grove Drive, Pasadena, CA 91109.
E-mail: stephens@atmos.colostate.edu

DOI: 10.1175/JCLI-D-11-00262.1

The more recent papers of Stephens (2005) and Stephens and Ellis (2008) describe yet another important aspect of the water vapor feedback that has largely been ignored. Changes to the radiation balance of the atmosphere in response to global warming control the change in global precipitation (Stephens and Hu 2010; Wild and Liepert 2010). These changes to the atmospheric balance occur as a result of changes to the low-level water vapor via two primary contributions; one due to changes in absorbed solar radiation and the second by changes in the emitted longwave radiation from the atmosphere to the surface [hereafter downwelling longwave radiation (DLR)]. Both are largely determined by the low-level water vapor.

The purpose of this paper is twofold. It is our intent to provide a review of our current state of understanding of the global, annual mean DLR as presented in the next section. The motivation here stems from the fact that there appears to be an unacceptable wide range of existing published values of this flux as discussed in the next section. Although the range in DLR given in the next section exceeds 20 W m^{-2}, there is good reason to eliminate a number of these estimates resulting in a much smaller range of values of both clear-sky and all-sky DLR and the related net longwave flux at the surface. We determine this range is approximately 6 W m^{-2} and the error (one sigma) is approximately ± 10 W m^{-2} mostly arising from uncertainties attached to atmospheric state data (temperature and water vapor) needed to compute the DLR as previously noted in other studies (e.g., Zhang et al. 1995; Garratt 2001; also section 4).

The second and related purpose of this study is to examine the factors that control the DLR, specifically quantifying the relation between DLR, water vapor, temperature, and clouds as a step toward understanding the main sources of uncertainty on the DLR as well as a step toward deciphering the source of model bias error, which is a topic of an ongoing study. The effects of clouds on the DLR are quantified in section 3 using new satellite observations that are introduced in section 2. From the analysis of these data we find that clouds increase the global, annual mean DLR in the range 24–34 W m^{-2} thus underscoring the fundamental contribution of clouds to the planet's greenhouse effect. The influence of temperature and water vapor on the DLR is then analyzed in section 4 via the introduction of a simple model of clear-sky DLR as used in other studies (Garratt 2001; Stephens and Hu 2010). The performance of this simple model is checked against surface flux observations collected from a few sites. This model is then used in section 5 to predict how the clear-sky DLR has likely changed over the period from 1987 to 2005.

2. Global, annual mean downward longwave radiation estimates

Table 1 summarizes various global mean estimates of surface DLR and are grouped into four main categories: one flux is inferred as a residual of the other fluxes of the surface energy budget, three different flux estimates derive from reanalaysis that we consider are chiefly model based, another estimate is from surface flux measurements from a number of different sites that are averaged to deduce a global value directly, and the fourth category of estimates is synthesis products that ingest global observations of key cloud and aerosol information as well as global temperature and humidity data to calculate the fluxes. These synthesis products have generally undergone extensive and direct evaluation with surface flux observations. These products also come with matched TOA fluxes that are either used as an additional constraint on the derived fluxes by forcing agreement to observed TOA fluxes or as an independent check on the procedure to derive the surface fluxes by comparison of calculated and observed TOA fluxes.

a. The residual flux estimate

Trenberth et al. (2009) provide a depiction of the earth's global energy budget for the Earth Radiation Budget Experiment (ERBE) and Clouds and the Earth's Radiant Energy System (CERES) satellite periods by synthesizing a variety of observations and model simulations where gaps exist in observations. This synthesis is an update to the study of Kiehl and Trenberth (1997) and is inferred as a residual of the surface energy balance with an arbitrary adjustment upward of approximately 10 W m^{-2} partly in recognition that the value-derived value without adjustment is more than 20 W m^{-2} lower than the International Satellite Cloud Climatology (ISCCP) flux value (discussed below) considered for comparison. The justification given for this arbitrary adjustment is that errors in DLR are considered substantially larger than errors in any of the other components of surface energy balance, although no quantitative uncertainties are placed on these other fluxes.

b. Surface flux measurements

Two surface-based databases established at the Swiss Federal Institute of Technology are also incorporated into the observational estimate given in Table 1. The data come from the Global Energy Balance Archive (GEBA; Ohmura et al. 1989) and Baseline Surface Radiation Network (BSRN; Ohmura et al. 1998) surface observations. The GEBA database provides worldwide measured energy fluxes at the earth's surface and contains monthly mean values of the various surface energy

TABLE 1. All-sky and clear-sky global, annual mean downward longwave fluxes in W m^{-2}. Uncertainties given as ± are determined from surface measurement validation (for surface radiation budget SRB) and from global average sensitivity studies. Asterisks indicate an incomplete estimate of error that accounts only for instrument error.

	All sky			Clear sky		
	LW up	LW down	LW net	LW up	LW down	LW net
Trenberth et al (2009), 2000–2004	396	333	−63			
Wild et al. 1998	397	345±>5*	−52	397	321.5±5	−75.5
Reanalysis						
NRA						
ERBE period (1985–1989)	395.5	334.1	−61.4		312.7	−84.7
CERES period (2000–04)	396.9	336.5	−60.4			
ERA-40						
ERBE	394.2	340.2	−54.2		314.1	−82.1
JRA						
ERBE	395.6	324.3	−71.3			
CERES	396.9	324.1	−72.8			
GEWEX SRB						
January 1984–December 2007)						
Primary	396.5	343.9±11	−52.6	395.9	310.4±11	−85.5
QC	398.7	347.5±13	−51.2		313.2±13	−85.5
ERBE						
February 1985–April 1989)						
Primary	395.9	343.7±11	−52.2	395.4	309.2	−86.2
QC	398.0	347.5±13	−50.4		312.0	−85.9
CERES						
March 2000–May 2004)						
Primary	397.2	343.7±11	−53.5	396.7	310.7	−86.0
QC	399.1	346.7±13	−52.3		313.3	−85.8
ISCCP–FD 1985–1989	395.6	344.7±10/15	−50.9	394.1	313.5±10/15	−80.6
CERES (Ed2 AVG) 2000–05	398.0	342.0	−56.0	397.3	315.2	−82.1
A-Train						
2006–09						
Radar (only)	398	334	−64			
Radar + lidar (*H*)	398±9	350±9	−48±9		326	−72
Radar + lidar [CERES, CALIPSO, *CloudSat*, and MODIS (CCCM)]	398±5	347.2±7	−51±9	396	313	−83

balance components. The BSRN database includes DLR measurements at high temporal resolution (minute values) with the highest possible accuracy at selected sites in different climate regions. Although the best-documented component in GEBA is the shortwave downward radiation (Gilgen et al. 1998), this database also contains a limited number of sites that provide DLR measurements as reported by Wild et al. (1995, 2001). Wild et al. (1998, 2001) combine data from a total of 45 GEBA–BSRN observation sites with information on model and reanalysis biases to derive a value of 345 W m^{-2}. The individual measurement uncertainty of the BSRN fluxes is approximately 5 W m^{-2}, although the uncertainty assigned to the global flux composite is much larger than this individual measurement error due to additional unknown representiveness errors.

c. *Reanalysis surface longwave fluxes*

Three different reanalysis sources are also summarized for two periods as in Trenberth et al. (2009), one corresponding to the ERBE period (February 1985–April 1989) and the second to the CERES period 2000–04. The three sources of data are the National Centers for Environmental Prediction (NCEP; Kalnay et al. 1996), the 40-yr European Centre for Medium-Range Weather Forecasts (ECMWF) Re-Analysis (ERA-40; Uppala et al. 2005) fluxes and the Japanese 25-yr reanalysis (JRA; Onogi et al. 2007).

d. *Synthesis flux data*

Four different synthesis products are summarized.

1) DLR from the National Aeronautics and Space Administration (NASA)/ Global Energy and Water Cycle Experiment (GEWEX) Surface Radiation Budget (SRB) project (http://gewex-srb.larc.nasa.gov, Stackhouse et al. 2011), which provides a long-term record of global gridded datasets for shortwave and longwave surface and TOA fluxes from July 1983 to December 2007. Also included are fluxes from the

ERBE and CERES time periods above. Two sets of flux data are included in this archive—one referred to as the primary product and a second derived from more empirically based methods referred to as the quality-check (QC) product . The primary longwave algorithm is adapted from Fu et al. (1997, 1998) with an updated water vapor continuum (Kratz and Rose 1999). The QC longwave algorithm is from Gupta et al. (1992, 2010). The cloud and surface reflectance and cloud radiative properties are provided by the International Satellite Cloud Climatology Project DX (ISCCP; Rossow and Schiffer 1999) dataset. Maximum cloud overlap is assumed for clouds with cloud top pressures within high (<440 mb), middle (440–680 mb), and low (>680 mb) cloud layers and random overlap between those three main layers. Fluxes are computed for each scenario and averaged according to their probability for each 3-hourly time period. Surface emissivities are assigned according to a $1° \times 1°$ surface cover maps as described in Wilber et al. (1999). Temperature and water vapor profiles are taken from the 6-hourly 4D data assimilation products provided by the Global Modeling and Assimilation Office (GMAO) and produced using Goddard Earth Observing System reanalysis (GEOS4, Bloom et al. 2005). The 3-hourly surface skin temperatures use GEOS4 and ISCCP retrieved skin temperatures. The fluxes from both suites of algorithms have been extensively compared to surface observations. These comparisons indicate that the mean biases are well within the uncertainty for given BSRN measurements (i.e., within 5 W m^{-2}) and random errors that arise from a variety of factors (but notably uncertainty in atmospheric state, i.e., Zhang et al. 2006) are ± 11 and ± 13 W m^{-2} for the primary and QC fluxes respectively.

2) ISCCP fluxes are from Zhang et al. (2004). These fluxes are calculated from an advanced radiation scheme using ISCCP–D1 input data that includes global observations of the key variables. These flux data are considered to be an improvement over earlier versions of the similar data (Zhang et al. 1995) having exploited the availability of a more advanced radiative transfer model and improved ISCCP cloud climatology and ancillary datasets. An 18-yr flux record at 3-h time steps, global at 280-km intervals has been created; included in this record are both full- and clear-sky, shortwave and longwave, upwelling and downwelling fluxes at five levels [surface (SRF), 680 mbar, 440 mbar, 100 mbar, and top of atmosphere (TOA)]. Based on comparisons of monthly, regional mean values to the ERBE and the CERES TOA fluxes and to BSRN surface fluxes, Zhang et al. conclude that the overall uncertainties are 5–10 W m^{-2} at TOA and 10–15 W m^{-2} at the surface.
3) The Surface longwave flux from the CERES Ed2 average (AVG) product is estimated using data from January 2001 through December 2004. The method of the flux calculations in AVG is given in Kato et al. (2011). Briefly, inputs for the AVG flux computations include the following: 6-hourly temperature and humidity profiles and 3-hourly skin temperature from GEOS4, and Moderate Resolution Imaging Spectroradiometer (MODIS) and 3-hourly geostationary satellites–derived cloud properties (Minnis et al. 2011) to account for the diurnal cycle. The fluxes are computed at TOA, surface, and three atmospheric pressure levels (500, 200, and 70 hPa). TOA fluxes are computed without constraining the flux by the CERES angular distribution model derived TOA flux.
4) Two different derived estimates of DLR based on the use of *CloudSat* and other A-train observations of cloudiness and atmospheric state parameters are other examples of synthesis products. One uses the updated version of the radiative flux product (2B-FLXHR) product (L'Ecuyer et al. 2008) that includes improved depictions of clouds through the combination of lidar and radar observations (Henderson et al. 2011, manuscript submitted to *J. Appl. Meteor. Climatol.*). Vertical distributions of liquid and ice cloud water contents and effective radii from the level-2 cloud water content product (2B-CWC) are combined with ancillary temperature and humidity profiles from the ECMWF analyses and surface albedo and emissivity data from the International Geosphere-Biosphere Programme (IGBP) global land surface classification to initialize a two-stream, doubling-adding broadband radiative transfer model. Details of the approach are provided in L'Ecuyer et al. (2008) and Henderson et al. (2011, manuscript submitted to *J. Appl. Meteor. Climatol.*). A noteworthy difference between this product and others like it is the radiative effects of precipitation are explicitly included using estimates of rainfall rate and the height of the raining column from the *CloudSat* precipitation (2C-PRECIP-COLUMN) product (Haynes et al. 2009). The updated version of 2B-FLXHR includes aerosols with optical properties derived from the Spectral Radiation-Transport Model for Aerosol Species (SPRINTARS) global aerosol transport model (Takemura et al. 2000, 2002, 2005) adjusted to match Cloud–Aerosol Lidar and Infrared Pathfinder Satellite Observations (CALIPSO) aerosol information.

The second A-Train flux product is that of Kato et al. (2011). This product also uses *Cloudsat* radar and

CALIPSO lidar profile data as well as other A-Train data including cloud properties taken from MODIS observations using the a CERES cloud algorithm (Minnis et al. 2008). Temperature and humidity profiles used in the computations were from the Goddard Earth Observing System (EOS) Data Assimilation System reanalysis (GEOS-5).

The all-sky DLR values listed in Table 1 vary from a low of 324 W m^{-2} to a high of 350 W m^{-2}. It is relevant to note that the different DLR estimates given apply to slightly different periods of time. However, the expectation is that the DLR increases with warming at a rate of about 0.15–0.25 W m^{-2} yr^{-1} (section 5) and thus the difference between estimates in the ERBE period and the A-Train period, for example, would account for only about 3 W m^{-2} of this range. The low JRA values are unrealistic (see discussion section 5). The Trenberth et al. (2009) estimate and the radar-only estimate derived from A-Train data are the other two low outliers that can also be rejected as unrealistic. The first of these lacks rigor in the way it is deduced and the radar only estimate includes effects of clouds only detected by the cloud radar (e.g., Haladay and Stephens 2009). These undetected clouds that impact the DLR are mostly low clouds and the degree of this impact can be judged by comparing the radar only and radar + lidar estimated DLR given in Table 1 (approximately 17 W m^{-2}). The other two reanalysis fluxes are also notably low compared to the synthesis fluxes that vary from 344 (GEWEX SRB) to 350 W m^{-2} (A-train). The surface upward longwave flux values from the sources reviewed range between 394 and 399 W m^{-2} and the net surface longwave flux varies over a range of values from −73.2 to −48 W m^{-2}. The clear-sky synthesis DLR fluxes vary between 309 and 326 W m^{-2} and this approximate 17 W m^{-2} range is larger than the all-sky range of synthesis flux values suggesting that one of the principle sources for the difference between all estimates is the different water vapor and temperature information used to produce the clear-sky flux values (see Zhang et al. 2006; also Garratt 2001).

The A-Train fluxes are especially noteworthy because, unlike the other estimates given in Table 1 and apart from the BSRN–GEBA observations of Wild et al. (2001, 2008), the flux values quoted are based on actual cloud profile observations, notably including the critical new information about cloud base derived from *CloudSat* and CALIPSO (Mace et al. 2009). Cloud-base information is one of the important parameters needed to determine the DLR under cloudy conditions (Stephens et al. 2002). The two different estimates of the DLR based on the blended lidar–radar observations of the A-Train differ only by 3 W m^{-2} despite the fact they use entirely different atmospheric state data and assumption about cloud properties.

The synthesis products also attach an independently deduced uncertainty to the fluxes that range between about 10 and 15 W m^{-2}. We consider that ±10 W m^{-2} is a reasonable estimate of the one-sigma error on global DLR.

3. Cloud influences on DLR

The effects of clouds on the DLR are examined first using the Henderson et al. (2011, manuscript submitted to *J. Appl. Meteor. Climatol.*) A-train data. These flux data are shown in Fig. 1 in the form of an annual mean map of the cloud and clear-sky DLR differences [bottom of atmosphere (BOA) cloud radiative effect (CRE), Fig. 1a]. The equivalent cloud minus clear-sky fluxes at the TOA (TOA CRE, Fig. 1b) are also shown for contrast, and the column water vapor derived from the Special Sensor Microwave Imager (SSM/I) data are provided for diagnostic purposes.

The BOA longwave CRE can be considered to be a measure of the greenhouse effect of clouds on the surface energy balance. According to the A-Train estimates of these flux differences inferred from Table 1, the global mean BOA CRE lies approximately in the range 24–34 W m^{-2} (Table 1), which is also consistent with the 31 W m^{-2} reported by Zhang et al. (2004). Such effects of clouds on the DLR are straightforward to understand and have been understood for some time. Clouds produce an additional source of emission to the surface increasing the DLR relative to clear-sky fluxes. Four main factors influence the magnitude of this increased emission: i) the height of cloud base, which approximately defines the temperature at which clouds emit radiation downward to the surface, ii) the opacity of the cloud itself that also defines the level at which the emission occurs within the cloud and thus the temperature of the emission, iii) the amount of water vapor that lies below cloud base that absorbs the cloud emitted radiation re-emitting at a different (warmer) temperature thereby reducing the sensitivity of the DLR to clouds (the water vapor opacity effect), and iv) the areal amount of cloud. Since global cloud-base information only became available with A-Train observations, estimates of global CRE at the surface prior to these A-Train observations were uncertain by an amount that could not be readily assessed.

Although expected, the contrast between the TOA and BOA CRE shown in Fig. 1 is nevertheless remarkable. It has been known since the first IR observations of clouds from space that the lowest emitting temperatures and thus largest values of TOA CRE occur from

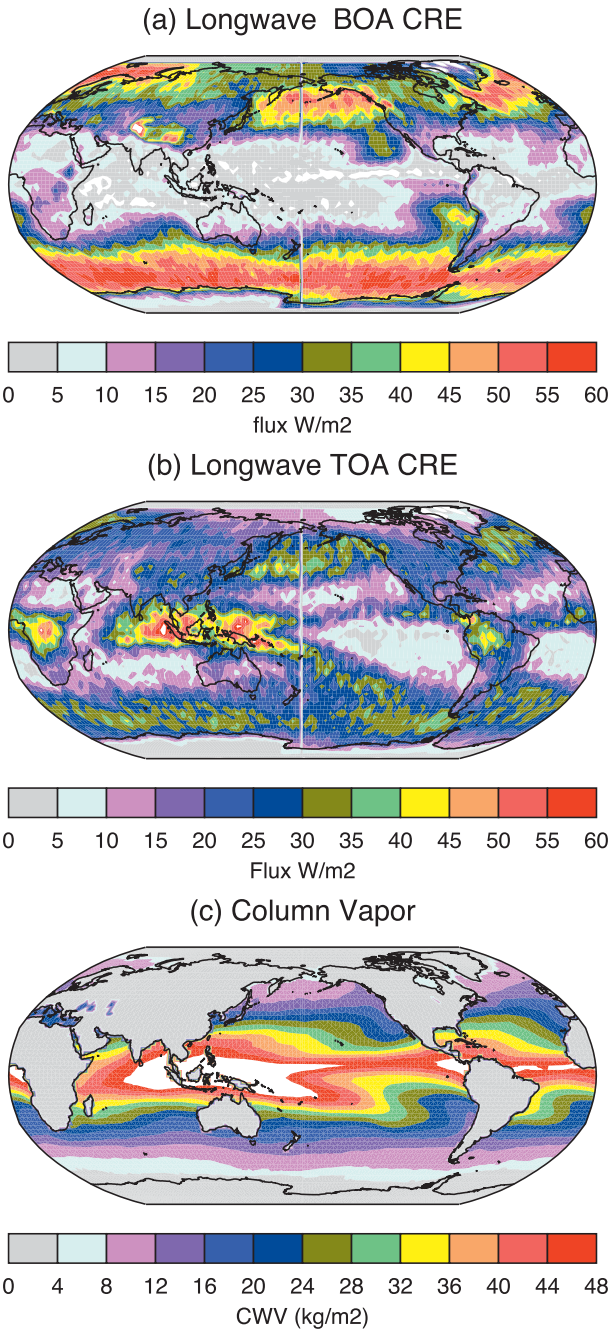

FIG. 1. The annual-mean distribution of (top) BOA CRE, (middle) TOA CRE, and (bottom) column water vapor. The flux data are an average of the A-Train observations collected over 2007, and the water vapor data are an 18-yr average from 1988 to 2005.

the coldest and highest cloud tops located in tropical latitudes. The BOA CRE, by contrast, is at a minimum in these lower latitudes because of the large water vapor burden below cloud base over the warmer tropical oceans. Thus a very different indication of the greenhouse effect of clouds emerges when considering BOA

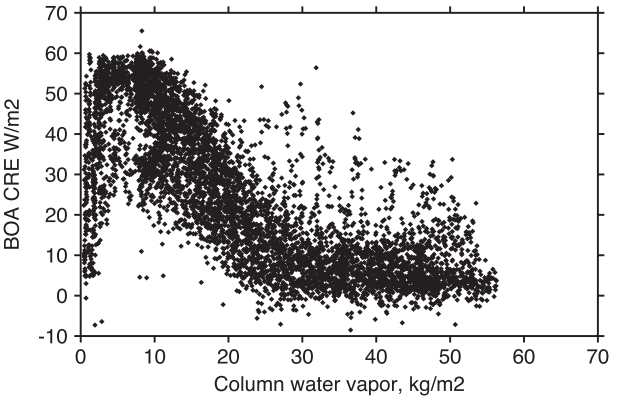

FIG. 2. The effect of clouds on the downwelling longwave flux at the earth's surface as a function of column water vapor.

effects rather than TOA effects on longwave fluxes. This opacity effect reveals itself in comparison of water vapor (Fig. 1c) to the CRE (Figs. 1a,b). The BOA CRE values are largest in the mid-to-high latitudes where the water vapor opacity effects are least and where the TOA CRE is, by contrast, smallest. The inverse correlation between the BOA CRE and column water vapor hinted at in Fig. 1 is more explicitly revealed in Fig. 2. For regions of water vapor above about 30 kg m^{-2} the opacity effect of the water vapor below cloud is so dominant that the DLR is largely independent of the emission from cloud base. The opacity effect systematically decreases as the water vapor decreases from about 30 kg m^{-2} resulting in a systematic increase of BOA CRE as the water vapor decreases.

4. The clear-sky DLR and net surface longwave fluxes

The influences of water vapor and atmospheric temperature on the DLR values listed in Table 1 are now investigated via the introduction of a very simple but accurate model of clear-sky DLR.

a. A simple model of the clear-sky DLR

The mutual importance of both the near-surface temperature and near-surface water vapor in governing the clear sky DLR at the earth's surface has been understood for almost a century. Angstrom (1918), Brunt (1932), and Elsasser (1942) each proposed that the downward irradiance could be represented in terms of the screen temperature and water vapor pressure of the air near the ground. Idso and Jackson (1969), Brutsaert (1975), and Prata (1996) further introduced parameterizations more appropriately in terms of that path-integrated information like precipitable water (PW) since this is the primary measure of the mass of the radiatively active gas. However, the broader availability of surface observations of

water vapor pressure and the difficulty in obtaining the PW at surface sites led these authors to adopt more pragmatic models that characterized the contribution by water vapor to this flux in terms of the more readily available surface measurements. Dilley and O'Brien (1998) introduced a pair of simple models of the clear-sky DLR, including a revision of the Swinbank (1963) formula, that predict the clear-sky DLR in terms of screen temperature and precipitable water.

Here we adopt the following Dilley and O'Brien model for clear-sky DLR,

$$\mathrm{DLR} = \alpha + \beta\left(\frac{T}{T_*}\right)^6 + \gamma\left(\frac{w}{w_*}\right)^{1/2}, \qquad (1)$$

which identifies two main contributions, one involving the near surface temperature T (in K) and the second involving the column water vapor w (in kg m^{-2}). The relevant constants in this expression are as follows: $T_* = 273.16$ K, $w_* = 25$ kg m^{-2}, $\alpha = 59.38$, $\beta = 113.7$, and $\gamma = 96.96$ W m^{-2}.

b. Comparison to BSRN data

The superiority of the model expressed by (1) over some of the earlier schemes mentioned above was demonstrated by Dilley and O'Brien (1998). They showed that the DLR predicted by (1) compared to detailed radiative transfer calculations with rms errors of approximately 5 W m^{-2}. This result is further confirmed here by comparison of the calculated DLR to measurements from a limited number of surface sites. The surface measurements of DLR are from three different BSRN oceanic (island) sites that provide a sufficiently long record (greater than 10 years). The restriction to oceanic sites was required to use both available satellite (microwave) water vapor data that are relevant over oceans and local sea surface temperature (SST) data to calculate the clear-sky DLR using (1). The gridded monthly mean SST data of Reynolds et al. (2002) and microwave water vapor data of Wentz (2006) located nearest each BSRN island site were used in this study. The requirement for decadal-in-length data provides an opportunity to evaluate the changes in DLR both calculated and observed that occur from interannual variations of the climate system. Both the restriction over oceans and a requirement for long time series limit the sources of data to just a few stations in the BSRN network.

The BSRN data were screened to identify clear-sky fluxes to compare to the calculated fluxes. The clear-sky screening approach adopted the following simple steps. The BSRN flux data are recorded at a time resolution of one minute. The maximum diurnally resolved measured solar flux at the surface was determined for each month at each time. This solar flux maximum was then assumed to represent a clear-sky reference condition for that month. Since clear-sky fluxes themselves have some variability over any given month, the times at which any instantaneous solar flux was measured within 5 W m^{-2} of the respective (instantaneous) clear-sky reference maxima were then flagged as times of clear skies. The longwave fluxes measured at these times were then accumulated to provide the monthly mean clear-sky longwave fluxes used for the comparison.

Figure 3 provides a comparison between the measured and calculated monthly mean clear-sky longwave fluxes of DLR. The comparisons reveal a remarkable degree of agreement between these two forms of flux both with respect to bias and variability. Biases range between 0.8 and 2 W m^{-2}, and the rms difference between observed and modeled fluxes varies between 2 and 3.4 W m^{-2} for the three sites chosen. This level of agreement is consistent with the Dilley and O'Brien (1998) assessment of their method.

c. Sensitivity of DLR to temperature and water vapor

The simple model described above provides a simple way of deducing the errors in the DLR from water vapor and temperature errors. Although such an analysis provides nothing new qualitatively given past sensitivity studies (e.g., Zhang et al. 2006), it does offer useful quantitative guidance on the magnitudes of errors of clear-sky fluxes. Assuming an error ΔT on temperature and error Δw on column water vapor, then it simply follows from (1) that the corresponding error in DLR is

$$\Delta\mathrm{DLR} = 6\beta\left(\frac{T}{T_*}\right)^5\frac{\Delta T}{T_*} + \frac{1}{2}\gamma\left(\frac{w}{w_*}\right)^{-1/2}\frac{\Delta w}{w_*}. \qquad (2)$$

For global mean conditions of approximately $T = 290$ K and $w = 28$ kg m^{-2}, it follows that the DLR = 319 W m^{-2} (also approximately in the midrange of clear-sky DLR given in Table 1). As noted in Garratt (2001) the first term of (2) yields a temperature sensitivity of 3.36 W m^{-2} K^{-1} and the second provides the sensitivity to water vapor of 1.94 W m^{-2} (kg m^{-2})$^{-1}$. Thus a 1–2° error in temperature and a 10% error in column water vapor equates to a 8.7–12.1 W m^{-2} error in clear-sky DLR. Since these are typical of errors in global temperature and water vapor, it follows that the characteristic error in clear-sky DLR is approximately 10 W m^{-2}.

In a different context Stephens and Hu (2010) employed a version of (2) to deduce how much the DLR would be expected to change given a prescribed amount of global warming. In this context the change in Δw is determined to first order by the change in ΔT through

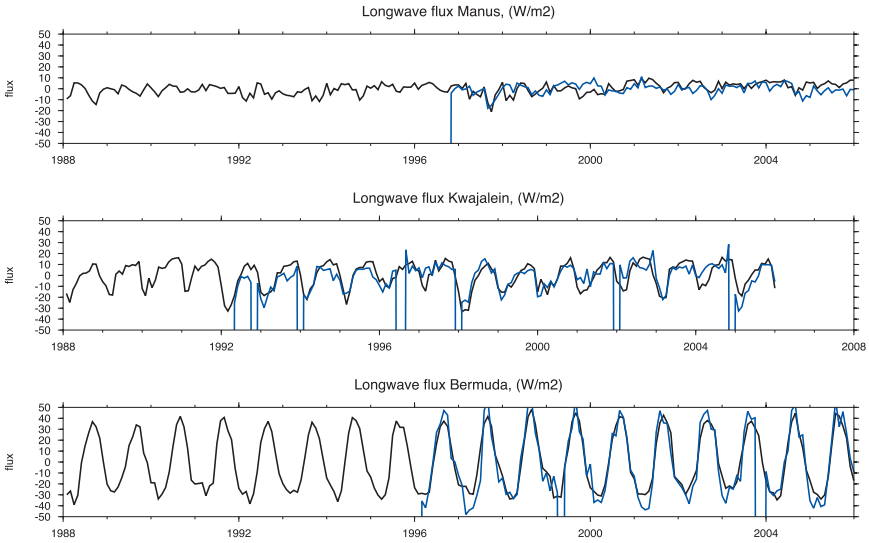

FIG. 3. A comparison of clear-sky-simulated DLR (refer to text) to DLR observed at three different BSRN sites. The simulated fluxes (solid line) are for an approximate 18-yr period whereas the observations (blue) are over a shorter period of time.

the Clausius–Clapeyron relation. If we assume that $(1/w)(dw/dT) = 0.07\,\mathrm{K}^{-1}$ as typically found in climate change simulations (e.g., Stephens and Ellis 2008 among others) then (2) becomes

$$\Delta\mathrm{DLR} = 6\beta\left(\frac{T}{T_*}\right)^5\frac{\Delta T}{T_*} + \frac{1}{2}\gamma\left(\frac{w}{w_*}\right)^{1/2}0.07\Delta T \quad (3)$$

leading to a sensitivity of 7.2 W m^{-2} K^{-1} warming. This almost exactly matches the rate of increase in DLR projected by the warming that occurs in global models (Stephens and Hu 2010).

5. The DLR and climate change

There are currently no global-wide observations of DLR yet all estimates of its change associated with global warming suggest that the DLR is likely to undergo the largest change of any of the other components of the planet's energy balance. The physical explanation for the heightened sensitivity of the DLR to warming lies in the fact that both a warming and moistening of the (lower) atmosphere, which themselves are mutually connected via the water vapor feedback, positively contribute to the increase in DLR. This response is unlike the response of the outgoing longwave radiation that occurs as net result of competing effects between moistening that lowers emission to space and warming that increases emission to space (Stephens 1999; Stephens and Hu 2010).

If we apply the oceanic-wide precipitable water and SST observations used to derive the clear-sky fluxes of section 3 for specific locations, then we can deduce the expected change in clear-sky DLR over the 18 years of observations (1988–2005) over the global oceans. The results of these calculations are highlighted in Fig. 4 showing the time series of 60°N/S-averaged column water vapor, SST, and clear-sky DLR contrasted against other similar estimates of DLR trend. The upward trend of approximately 0.18 K decade^{-1} in SST and the upward trend in satellite water vapor data of 0.40 mm decade^{-1} in the version-6 release data used here are discussed in Trenberth et al. (2007). The trend in the clear-sky DLR found over the oceans, based on a linear fit to the time series, is 1.8 ±0.3 W m^{-2} decade^{-1}. Thus over the 18 years of the record analyzed the expected change in global oceanic DLR is 3.2 W m^{-2}, which is the same order of magnitude as the error obtained in calculating it (approximately 2–3 W m^{-2} according to the results of Fig. 3). Thus we conclude this trend in global-mean DLR would not yet detectible from observations.

A number of different estimates of the DLR trend also have recently been published, and these are summarized in Fig. 5 together with the current estimate of this study. The Prata (2008) estimate uses a globally distributed 25-yr record of radiosonde data to quantify the effects of the observed global increases in both surface air temperature and precipitable water on the clear-sky DLR. Based on the data used in that study, the surface air temperature increased by +0.22 K decade^{-1} and the precipitable water increased by +0.29 mm decade^{-1},

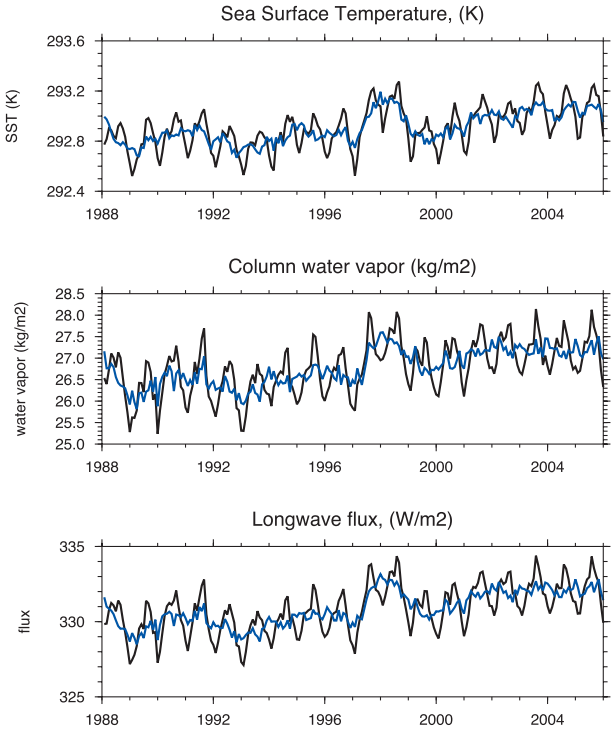

FIG. 4. (bottom) The global oceanic mean clear-sky longwave flux constructed from 18 years (1988–2005) of (top) SST and (middle) column water vapor. All sources of data used in this construction are described in the text. With the annual cycle removed (solid blue curves), trends in all quantities were calculated and are reported in the text. The inferred trend in oceanic-mean DLR is approximately 1.8 W m^{-2} $decade^{-1}$.

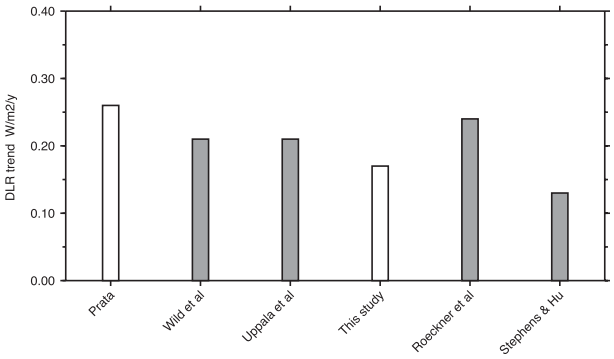

FIG. 5. A summary of DLR trends from various sources (refer to text), including the trend inferred from Fig. 4. All-sky DLR trends are shaded, and clear-sky trends are unshaded.

much less than that observed over oceans. This resulted in a calculated increase of downward clear-sky flux of approximately +1.7 W m^{-2} $decade^{-1}$ (0.17 W m^{-2} yr^{-1}) for the period 1964–90 and a slightly higher estimate (0.26 W m^{-2} yr^{-1}) based on surface observations for the later period 1992–2002 with more apparent moistening. Wild et al. (2008) estimate a trend in the all-sky DLR of 0.21 W m^{-2} yr^{-1} for the period 1986–2000 based on different sources and an estimate of 0.26 W m^{-2} yr^{-1} based on 12 BSRN stations covering a latitude range from polar to tropical regions for the period 1992–2000. ERA-40 also exhibits an increase in all-sky DLR of 0.21 W m^{-2} yr^{-1} between 1986 and 2000 (Uppala et al. 2005).

These estimates of trend are similar to the surface thermal fluxes simulated in a transient GCM experiment (Roeckner et al. 1999), from which Wild et al. infer an increase of all-sky 0.24 W m^{-2} yr^{-1} over global mean land surfaces and 0.25 W m^{-2} yr^{-1}, for data averaged over the same locations as the 12 BSRN stations used in Wild et al. (2008).

These results can also be placed in the context of climate change experiments performed with climate models. Stephens and Hu (2010) analyze data from the transient CO_2 climate change experiments of climateprediction.net based on a version of the Hadley center coupled ocean–atmospheric model [third climate configuration of the Met Office Unified Model (HadCM3)]. The analysis presented uses outputs from 1380 different models with perturbed parameterizations of physical processes. The results of these transient CO_2 experiments lead to change of 7 W m^{-2} K^{-1} as noted above, which is equivalent to a trend of 0.13 W m^{-2} yr^{-1} given the observed trend in SST. Stephens and Hu (2010) were also able to show how the change in DLR at the surface is approximately equally split between the increased temperature and increased moisture that occurred in these experiments. The study also showed how well the simple clear-sky DLR model of Dilley and O'Brien was able to fit the model predicted changes to all-sky DLR suggesting that it is the change in clear-sky DLR that largely determines the change in all-sky DLR in the climate change experiments of climateprediction.net.

6. Summary and conclusions

A number of sources of data that provide global, annual mean estimates of the downwelling longwave flux to the surface are reviewed including two new estimates derived from combinations of A-Train observations. The fluxes reviewed group into four main categories: i) a residual estimate that closes the surface energy balance assuming all other surface fluxes, ii) flux values compiled from global models used in reanalysis, iii) an average of surface observations from a limited number of surface sites, and iv) syntheses of global observations applied to radiation models. The latter flux estimates are typically assessed against surface observations and come with estimated errors. These synthesis fluxes also include matching TOA fluxes that serve as an independent, albeit

indirect, evaluation of the estimation process when matched to TOA flux measurements from satellite observations.

The main findings of the study are as follows.

(i) The range in values of global-mean DLR from the sources reviewed is 26 W m^{-2}. This range is summarized in Fig. 6. The values of DLR group into two main ranges, one between 344 and 350 W m^{-2}, which includes all synthesis values as well as the observational estimate from GEBA–BSRN and the second group of values range between 324 and 338 W m^{-2} mainly based on model estimates.

(ii) Given that the synthesis fluxes have been assessed against observations both at the surface and at the TOA, and given that formal error estimates are associated with them, the global-mean values from these fluxes products are thus deemed to be the most representative of the actual global-mean DLR of all four different categories of values reviewed. Thus we assert that the most likely value of DLR approximately lies in the range 345–350 W m^{-2} with an error of approximately ±10 W m^{-2}. The averages of BSRN surface flux observations also fall within this range of values as noted in Fig. 6.

(iii) For every degree error in temperature, the resultant clear-sky DLR error is 3.4 W m^{-2} and for every percentage error in column water vapor, the error in DLR is approximately 0.7 W m^{-2}. This sensitivity implies that the clear-sky error of the DLR is of order 10 W m^{-2} given typical errors in global sources of temperature and water vapor. The implication is that much of the uncertainties in estimating DLR as determined for the synthesis flux products revolve around estimation of the clear-sky emission and, by implication, the atmospheric state that determines this emission (e.g., Zhang et al. 1996; Zhang et al. 2006; Wild et al. 2001).

(iv) When compared to global models, Wild et al. (2001) find that model values of DLR are significantly lower than observations by as much as 10–20 W m^{-2}. For example, the intermodel mean of the Intergovernmental Panel on Climate Change (IPCC) Assessment Report 4 (AR4) models is 338 W m^{-2} (Wild 2008), where differences are most apparent in cold, dry conditions that correspond to where cloud effects on DLR are most pronounced (Figs. 1a and 2) suggesting that one possible source of model bias may be associated with model clouds. Garratt (2001) finds that the clear-sky DLR agrees with observations to the extent that the column water vapor of models also agrees with observations and generally there are not the systematic differences in clear-sky DLR as found in all-sky DLR, again implicating clouds as a possible source of discrepancy. In this study we also find the reanalysis all-sky fluxes are significantly lower than that from DLR synthesis. Thus we conclude that a bias of approximately 10 W m^{-2} exists in climate model–derived DLR and even larger differences are found with respect to global models used to produce reanalysis climate data. Although it is possible that clouds are the source of bias, the quantitative character and sources of these differences require more detailed study.

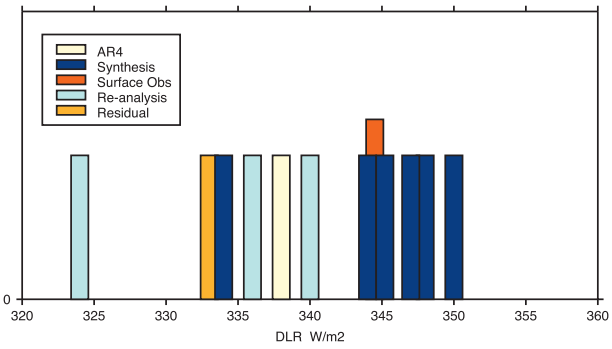

FIG. 6. A summary of the different estimates of global, annual mean all-sky DLR grouped according to the different categories of estimates described in the text.

(v) We show that a simple model of clear-sky DLR is able to match surface measurements of clear-sky fluxes within a bias of 1–2 W m^{-2} and an rms error of 2–3 W m^{-2}. However, the robustness of this result requires further testing with other sources of surface measurements. When applying such a model to 18 years of satellite observations of column water vapor and sea surface temperature, a trend in clear-sky DLR over the ocean regions between 60°S–N of 0.18 ±0.03 W m^{-2} yr^{-1} is obtained that falls in the middle of the published range of all-sky DLR trend varies from 0.13 to 0.26 W m^{-2} yr^{-1}. At present, these trends are barely discernible above the errors inherent to the procedures that produce them.

(vi) The effects of clouds on the DLR are also examined using flux data from one of the A-train products. The new observations of the A-Train provide the important information about cloud base that enables a more direct estimate of these effects. The BOA global-mean longwave cloud radiative effect (CRE, a difference between all sky and clear sky fluxes), a measure of the greenhouse effect of clouds on the surface energy balance, is estimated to be approximately 24–34 W m^{-2}. The BOA CRE

is shown to be strongly modulated by the underlying water vapor (we term the water vapor opacity effect) that gives rise to the maximum cloud sensitivities of the DLR as occurring in the colder drier regions of the planet, in direct contrast to the TOA CRE, which is maximum in regions of deepest and coldest clouds in the tropics.

The broader implications of this study are that our current depictions of the surface energy balance require significant revision. Significantly more flux of longwave radiation to the surface, in excess of 10 W m^{-2} compared to existing surface energy balance studies, requires an equivalent adjustment of other fluxes of heat from the surface to the atmosphere for balance. Study of the energy closure in light of the results of this study is underway.

Acknowledgments. NCEP reanalysis data provided by the NOAA/OAR/ESRL PSD, Boulder, Colorado, from their website at http://www.esrl.noaa.gov/psd/. This work was supported by the NASA Grants NNX07AR11G, NAS5-99237, and NNX09AK02G.

REFERENCES

Angstrom, A., 1918: A study of the radiation of the atmosphere. *Smithson. Misc. Collect.,* **65,** 1–159.

Arrenhius, S., 1896: On the influence of carbonic acid in the air on the temperature of the ground. *Philos. Mag.,* **41,** 237–276.

Bloom, S. A., and Coauthors, 2005: Documentation and validation of the Goddard Earth Observing System (GEOS) data assimilation system version 4. GEOS Tech. Rep. Series on Global Modeling and Data Assimilation 104606, 26 pp.

Brunt, D., 1932: Notes on radiation in the atmosphere. *Quart. J. Roy. Meteor. Soc.,* **58,** 389–418.

Brutsaert, W., 1975: On a derivable formula for long-wave radiation from clear skies. *Water Resour. Res.,* **11,** 742–744.

Callendar, G. S., 1938: The artificial production of CO_2 and its influence on temperature. *Quart. J. Roy. Meteor. Soc.,* **64,** 223–237.

Dilley, A. C., and D. M. O'Brien, 1998: Estimating downward clear sky long-wave irradiance at the surface from screen temperature and precipitable water. *Quart. J. Roy. Meteor. Soc.,* **124A,** 1391–1401.

Elsasser, W. M., 1942: *Heat Transfer by Infrared Radiation in the Atmosphere.* Harvard Meteorological Studies Series, Vol. 6, Harvard University Press, 87 pp.

Fu, Q., K.-N. Liou, and A. Grossman, 1997: Multiple scattering parameterization in thermal infrared radiative transfer. *J. Atmos. Sci.,* **54,** 2799.

——, P. Yang, and W. B. Sun, 1998: An accurate parameterization of the infrared radiative properties of cirrus clouds for climate models. *J. Climate,* **11,** 2223–2237.

Garratt, J. R., 2001: Clear-sky longwave irradiance at the earth's surface—Evaluation of climate models. *J. Climate,* **14,** 1647–1670.

——, D. M. O'Brien, M. R. Dix, J. M. Murphy, G. L. Stephens, and M. Wild, 1999: Surface radiation fluxes in transient climate simulations. *Global Planet. Change,* **20,** 33–55.

Gilgen, H., M. Wild, and A. Ohmura, 1998: Means and trends of shortwave irradiance at the surface estimated from Global Energy Balance Archive data. *J. Climate,* **11,** 2042–2061.

Gupta, S. K., W. L. Darnell, and A. C. Wilber, 1992: A parameterization for longwave surface radiation from satellite data: Recent improvements. *J. Appl. Meteor.,* **31,** 1361–1367.

——, D. P. Kratz, P. W. Stackhouse, A. C. Wilber, T. Zhang, and V. E. Sothcott, 2010: Improvement of surface longwave flux algorithms used in CERES processing. *J. Appl. Meteor. Climatol.,* **49,** 1579–1589.

Haladay, T., and G. Stephens, 2009: Characteristics of tropical thin cirrus clouds deduced from joint *CloudSat* and CALIPSO observations. *J. Geophys. Res.,* **114,** D00A25, doi:10.1029/2008JD010675.

Haynes, J. M., T. S. L'Ecuyer, G. L. Stephens, S. D. Miller, C. Mitrescu, N. B. Wood, and S. Tanelli, 2009: Rainfall retrieval over the ocean with spaceborne W-band radar. *J. Geophys. Res.,* **114,** D00A22, doi:10.1029/2008JD009973.

Held, I., and B. Soden, 2000: Water vapor feedback and global warming. *Annu. Rev. Energy Environ.,* **25,** 441–475.

Idso, S. B., and R. D. Jackson, 1969: Thermal radiation from the atmosphere. *J. Geophys. Res.,* **74,** 5397–5403.

Kalnay, E., and Coauthors, 1996: The NCEP/NCAR 40-Year Reanalysis Project. *Bull. Amer. Meteor. Soc.,* **77,** 437–471.

Kasting, J. F., 1989: Runaway and moist greenhouse atmospheres and the evolution of Earth and Venus. *Icarus,* **74,** 472–494.

Kato, S., and Coauthors, 2011: Improvements of top-of-atmosphere and surface irradiance computations with CALIPSO-, CloudSat-, and MODIS-derived cloud and aerosol properties. *J. Geophys Res.,* **116,** D19209, doi:10.1029/2011JD016050.

Kiehl, J. T., and K. E. Trenberth, 1997: Earth's annual global mean energy budget. *Bull. Amer. Meteor. Soc.,* **78,** 197–208.

Kratz, D. P., and F. G. Rose, 1999: Accounting for molecular absorption within the spectral range of the CERES window channel. *J. Quant. Spectrosc. Radiat. Transfer,* **61,** 83–95.

L'Ecuyer, T. S., N. B. Wood, T. Haladay, G. L. Stephens, and P. W. Stackhouse Jr., 2008: Impact of clouds on the atmospheric heating based on the R04 *CloudSat* fluxes and heating rates data set. *J. Geophys. Res.,* **113,** D00A15, doi:10.1029/2008JD009951.

Lindzen, R. S., 1990: Some coolness concerning global warming. *Bull. Amer. Meteor. Soc.,* **71,** 288–299.

Mace, G. G., Q. Zhang, M. Vaughn, R. Marchand, G. Stephens, C. Trepte, and D. Winker, 2009: A description of hydrometeor layer occurrence statistics derived from the first year of merged *CloudSat* and CALIPSO data. *J. Geophys. Res.,* D22306, **113,** doi:10.1029/2007JD009775.

Minnis, P., and Coauthors, 2008: Cloud detection in non-polar regions for CERES using TRMM VIRS and *Terra* and *Aqua* MODIS data. *IEEE Trans. Geosci. Remote Sens.,* **46,** 3857–3884.

——, and Coauthors, 2011: CERES edition-2 cloud property retrievals using TRMM VIRS and *Terra* and *Aqua* MODIS data. Part I: Algorithms. *IEEE Trans. Geosci. Remote Sens.,* **49,** 4374–4400, doi:10.1109/TGRS.2011.2144601.

Ohmura, A., H. Gilgen, and M. Wild, 1989: Global energy balance archive GEBA, World Climate Program project A7—Water, report 1: Introduction. Zuercher Geografische Schriften 34, Verlag der Fachvereine, Zuerich, 62 pp.

——, and Coauthors, 1998: Baseline Surface Radiation Network (BSRN/WCRP): A new precision radiometry for climate research. *Bull. Amer. Meteor. Soc.,* **79,** 2115–2136.

Onogi, K., and Coauthors, 2007: The JRA-25 Reanalysis. *J. Meteor. Soc. Japan,* **85,** 369–432.

Paltridge, G. W., A. Arking, and M. Pook, 2009: Trends in middle- and upper-level tropospheric humidity from NCEP reanalysis. *Theor. Appl. Climatol.,* **98,** 351–359, doi:10.1007/s00704-009-0117-x.

Prata, A. J., 1996: A new long-wave formula for estimating downward clear-sky radiation at the surface. *Quart. J. Roy. Meteor. Soc.,* **122,** 1127–1151.

——, 2008: The climatological record of clear-sky longwave radiation at the Earth's surface: Evidence for water vapour feedback? *Int. J. Remote Sens.,* **29,** 5247–5263.

Reynolds, R. W., N. A. Rayner, T. M. Smith, D. C. Stokes, and W. Wang, 2002: An improved in situ and satellite SST analysis for climate. *J. Climate,* **15,** 1609–1625.

Roeckner, E., L. Bengstssonn, J. Feichter, J. Lelieveld, and H. Rodhe, 1999: Transient climate change simulations with a coupled atmosphere–ocean GCM including the tropospheric sulfur cycle. *J. Climate,* **12,** 3004–3032.

Rossow, W. D., and R. Schiffer, 1999: Advances in understanding clouds from ISCCP. *Bull. Amer. Meteor. Soc.,* **80,** 2261–2287.

Santer, B. D., and Coauthors, 2007: Identification of human-induced changes in atmospheric moisture content. *Proc. Natl. Acad. Sci. USA,* **104,** 15 248–15 253, doi:10.1073/pnas.0702872104.

Shine, K. P., and A. Sinha, 1991: Sensitivity of the earths's climate to height dependent changes in the water vapor mixing ratio. *Nature,* **354,** 382–382.

Soden, B. J., D. L. Jackson, V. Ramaswamy, D. Schwarzkopf, and X. Huang, 2005: The radiative signature of upper tropospheric moistening. *Science,* **10,** 841–844.

Stackhouse, P. W., Jr., S. K. Gupta, S. J. Cox, T. Zhang, J. C. Mikovitz, and L. M. Hinkelman, 2011: The NASA/GEWEX surface radiation budget release 3.0: 24.5-Year Dataset. *GEWEX News,* No. 21, International GEWEX Project Office, Silver Spring, MD, 10–12.

Stephens, G. L., 1999: Radiative effects of clouds and water vapor. *Global Energy and Water Cycles,* K. A. Browning and R. J. Gurney, Eds., Cambridge University Press, 71–90.

——, 2005: Cloud feedbacks in the climate system: A critical review. *J. Climate,* **18,** 237–273.

——, and T. J. Greenwald, 1991: The earth's radiation budget and its relation to atmospheric hydrology. 1. Observations of the clear sky greenhouse effect. *J. Geophys. Res.,* **96,** 15 311–15 324.

——, and T. D. Ellis, 2008: Controls of global-mean precipitation increases in global warming GCM experiments. *J. Climate,* **21,** 6141–6155.

——, and Y. Hu, 2010: Are climate-related changes to the character of global precipitation predictable? *Environ. Res. Lett.,* **5,** 025209, doi:10.1088/1748-9326/5/2/025209.

——, and Coauthors, 2002: The *CloudSat* mission and the A-Train. *Bull. Amer. Meteor. Soc.,* **83,** 1771–1790.

Swinbank, W. C., 1963: Long-wave radiation from clear skies. *Quart. J. Roy. Meteor. Soc.,* **89,** 339–348.

Takemura, T., H. Okamoto, Y. Maruyama, A. Numaguti, A. Higurashi, and T. Nakajima, 2000: Global three-dimensional simulation of aerosol optical thickness distribution of various origins. *J. Geophys. Res.,* **105,** 17 853–17 873.

——, T. Nakajima, O. Dubovik, B. N. Holben, and S. Kinne, 2002: Single-scattering albedo and radiative forcing of various aerosol species with a global three-dimensional model. *J. Climate,* **15,** 333–352.

——, T. Nozawa, S. Emori, T. Y. Nakajima, and T. Nakajima, 2005: Simulation of climate response to aerosol direct and indirect effects with aerosol transport-radiation model. *J. Geophys. Res.,* **110,** D02202, doi:10.1029/2004JD005029.

Trenberth, K. E., and Coauthors, 2007: Observations: Surface and atmospheric climate change. *Climate Change 2007: The Physical Science Basis,* S. Solomon et al., Eds., Cambridge University Press, 235–336.

——, J. T. Fasullo, and J. Kiehl, 2009: Earth's global energy budget. *Bull. Amer. Meteor. Soc.,* **90,** 311–324.

Uppala, S. M., and Coauthors, 2005: The ERA-40 Re-Analysis. *Quart. J. Roy. Meteor. Soc.,* **131,** 2961–3012.

Wentz, F. J., cited 2006; Version-6 over-ocean product of Remote Sensing Systems. [Available online at http://www.remss.com.]

Wilber, A. C., D. P. Kratz, and S. K. Gupta, 1999: Surface emissivity maps for use in satellite retrievals of longwave radiation. NASA Tech. Rep. L-17861, NAS 1.60:209362, NASA/TP-1999-209362, 35 pp.

Wild, M., 2008: Short-wave and long-wave surface radiation budgets in GCMs: A review based on the IPCC AR4/CMIP3 models. *Tellus,* **60A,** 932–945.

——, and B. Liepert, 2010: The earth radiation balance as driver of the global hydrological cycle. *Environ. Res. Lett.,* **5,** 025203, doi:10.1088/1748-9326/5/2/025203.

——, A. Ohmura, H. Gilgen, and E. Roeckner, 1995: Validation of GCM simulated radiative fluxes using surface observations. *J. Climate,* **8,** 1309–1324.

——, ——, ——, ——, M. Giorgetta, and J. J. Morcrette, 1998: The disposition of radiative energy in the global climate system: GCM versus observational estimates. *Climate Dyn.,* **14,** 853–869.

——, ——, ——, J. J. Morcrette, and A. Slingo, 2001: Evaluation of downward longwave radiation in general circulation models. *J. Climate,* **14,** 3227–3239.

——, J. Grieser, and C. Schär, 2008: Combined surface solar brightening and greenhouse effect support recent intensification of the global land-based hydrological cycle. *Geophys. Res. Lett.,* **35,** L17706, doi:10.1029/2008GL034842.

Zhang, Y.-C., W. B. Rossow, and A. A. Lacis, 1995: Calculation of surface and top of atmosphere radiative fluxes from physical quantities based on ISCCP data sets: 1. Method and sensitivity to input data uncertainties. *J. Geophys. Res.,* **100,** 1149–1165.

——, ——, ——, V. Oinas, and M. I. Mishchenko, 2004: Calculation of radiative fluxes from the surface to top of atmosphere based on ISCCP and other global data sets: Refinements of the radiative transfer model and the input data. *J. Geophys. Res.,* **109,** D19105, doi:10.1029/2003JD004457.

——, ——, and P. W. Stackhouse Jr., 2006: Comparison of different global information sources used in surface radiative flux calculation: Radiative properties of the near-surface atmosphere. *J. Geophys. Res.,* **111,** D13106, doi:10.1029/2005JD006873.